nature nanotechnology

LETTERS

PUBLISHED ONLINE: 30 JUNE 2013 | DOI: 10.1038/NNANO.2013.118

Silicon chips detect intracellular pressure changes in living cells

Rodrigo Gómez-Martínez[1], Alberto M. Hernández-Pinto[2], Marta Duch[1], Patricia Vázquez[2], Kirill Zinoviev[1], Enrique J. de la Rosa[2], Jaume Esteve[1], Teresa Suárez[2] and José A. Plaza[1]*

The ability to measure pressure changes inside different components of a living cell is important, because it offers an alternative way to study fundamental processes that involve cell deformation[1]. Most current techniques such as pipette aspiration[2], optical interferometry[3] or external pressure probes[4] use either indirect measurement methods or approaches that can damage the cell membrane. Here we show that a silicon chip small enough to be internalized into a living cell can be used to detect pressure changes inside the cell. The chip, which consists of two membranes separated by a vacuum gap to form a Fabry–Pérot resonator, detects pressure changes that can be quantified from the intensity of the reflected light. Using this chip, we show that extracellular hydrostatic pressure is transmitted into HeLa cells and that these cells can endure hypo-osmotic stress without significantly increasing their intracellular hydrostatic pressure.

Scientific interest in the intersection of micro- and nanotechnologies with biology has focused on providing new tools to study fundamental questions in cell biology[5–7]. Fabrication based on these techniques offers the potential to develop integrated devices with nanosized moving parts[8] and allows for new opportunities for the mechanical analysis of cells[1,9,10]. However, the use of the devices has been focused on extracellular or invasive techniques[11]. Micro- and nanoparticles can be internalized inside living cells and have been used in numerous studies in cell biology. Furthermore, silicon-based particles have revealed their superiority in biological imaging and drug delivery because of their inherent biocompatibility[12,13]. Recently, for the purposes of single-cell labelling, we demonstrated a technique for the fabrication of silicon microparticles based on semiconductor technologies[14,15]. Using chemical functionalization, we also proved that these microparticles could react with the intracellular medium[16].

Existing techniques for the indirect measurement of intracellular pressure include methods that induce a large deformation of the cell by aspiration[2], or methods that detect variations in the cell volume[1,3]. In contrast, the servo-null technique allows for a direct measurement by inserting a micropipette as a pressure probe[4], but in this process the cell membrane is mechanically damaged. Thus, the measurement of extracellular loads transmitted to the interior of the cell, and in particular to a subcellular component, has not been demonstrated directly. Indeed, the cell is a highly complex and virtually unexplored mechanical system in which the membranes, cytoskeleton and extracellular matrix provide structural integrity.

Here, we have fabricated a nanomechanical chip that can be internalized to detect intracellular pressure changes within living cells, enabling an interrogation method based on confocal laser scanning microscopy (CLSM). The design comprises a mechanical sensor (Fig. 1a) defined by two membranes separated by a vacuum gap, and an optical reference area. The membranes act as parallel reflecting mirrors, constituting a Fabry–Pérot resonator that is partially transparent for some wavelengths[17]. An external pressure P deflects the membranes and changes the gap, t_{gap} (Fig. 1b). Accordingly, the intensity of the reflected light at the centre of the membranes, I_{r_Centre}, for a given wavelength λ, is modulated by P. The reference area is used for focusing purposes. Briefly, the sensing principle is based on the acquisition of images for a given λ and the quantification of I_{r_Centre}.

The fabrication processes included the deposition of three structural and three sacrificial layers, poly-silicon and silicon oxide, respectively (Fig. 1c, Supplementary Fig. S1). Polycrystalline silicon was selected as the structural material because of its elastic behaviour and high reliability[18]. The lateral dimensions of the mechanical membranes were fixed to 3 μm × 3 μm (Fig. 1d). Analytical and simulated analyses showed that the mechanical deformation was highly dependent on the membrane thickness and the linear response versus P (Fig. 1e, Supplementary Fig. S2). We therefore selected 50-nm-thick membranes to achieve a theoretical mechanical sensitivity of 5.5 nm per bar. The high refraction index of poly-silicon gives a spectral selectivity to the structure and, subsequently, a high sensitivity to P. Theoretically, the optical reflection of the structure (Fig. 1f) showed a resonance valley that was a function of t_{gap} and λ (Fig. 1g,h). Thus, P shifted the reflection curve towards smaller values ($\sim 2 \times \Delta t_{gap}$) and, for fixed λ, large variations in the reflection could be obtained. Finally, $t_{gap} \approx 300$ nm was selected by considering the high optical sensitivity and cell internalization capabilities.

The fabricated devices were validated using a bright-field optical microscope. The experiment showed a minimum reflection for $\lambda \approx 570$ nm (Fig. 2a). For fixed λ, I_{r_Centre} increased versus P for $\lambda > 580$ nm, and decreased for $\lambda < 560$ nm. CLSM images with superior resolution allowed an image-processing algorithm to be developed to detect the pressure loads based on a quantification of the mean intensities of three regions of interest (Supplementary Figs S3–S5). External pressure was applied from 0 to 1 bar and from 1 to 0 bar. I_{r_Sensor} decreased with a laser wavelength of 514 nm and increased with 594 nm (Fig. 2b).

To test the sensor inside living cells, we took advantage of our previous experience of internalizing silicon microparticles inside HeLa cells by lipofection[16]. Sensors were easily localized by optical light microscopy because of the higher reflectivity of the poly-silicon, and CLSM showed the specific location of the chip in the cytoplasm (Fig. 3a,b). The internalized sensors only represented 0.2% of the total volume of a typical HeLa cell (Supplementary Fig. S6). After transfection, a number of HeLa cells in the culture displayed vacuoles as a result of the lipofection procedure. Our experiments showed that these vacuoles did not affect cell fitness or viability (Fig. 3a,b,

[1]Instituto de Microelectrónica de Barcelona, IMB-CNM (CSIC), Esfera UAB, Campus UAB, 08193, Cerdanyola, Barcelona, Spain, [2]Centro de Investigaciones Biológicas, CIB (CSIC), C/Ramiro de Maeztu 9, 28040, Madrid, Spain. *e-mail: joseantonio.plaza@imb-cnm.csic.es

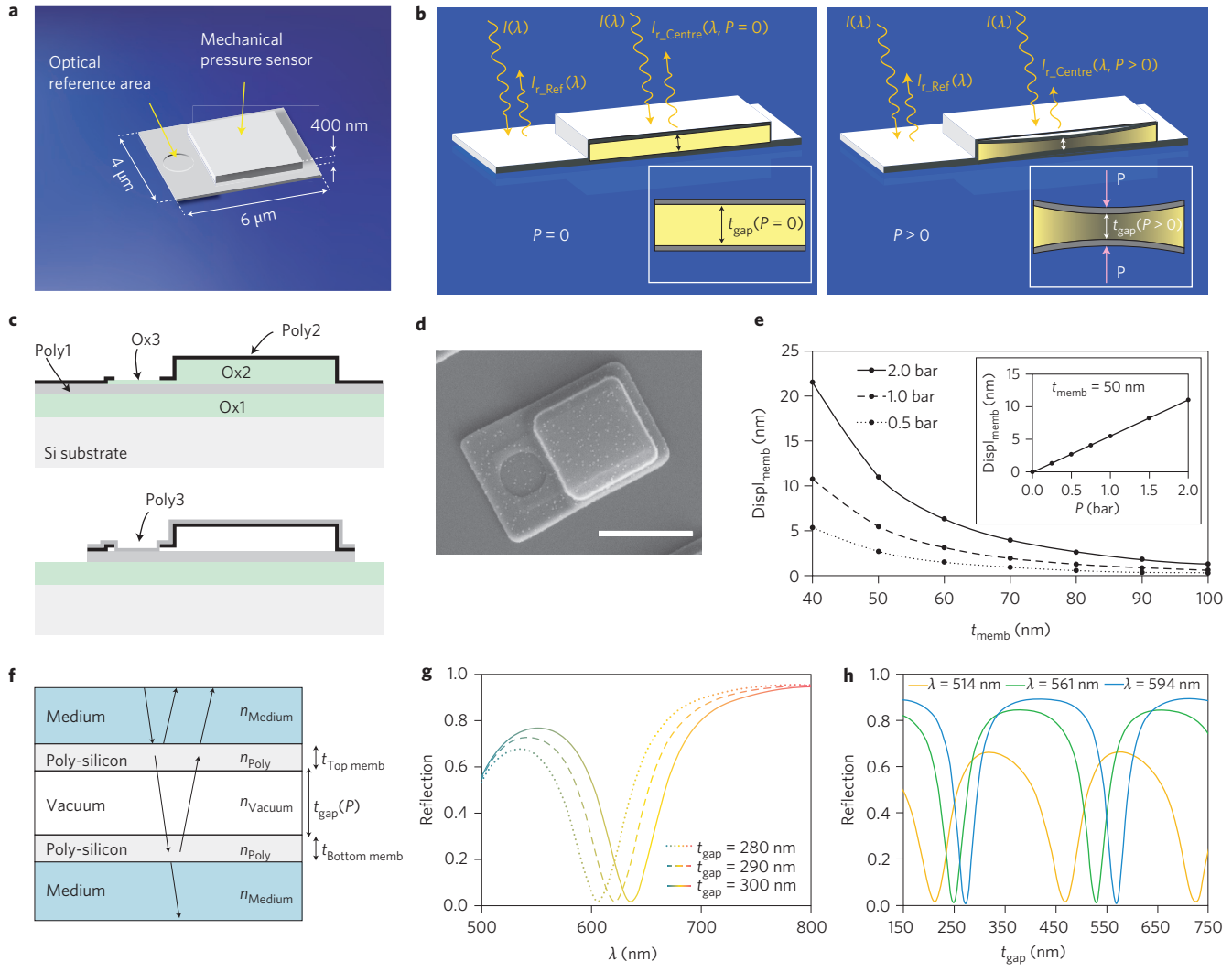

Figure 1 | Design and sensing principle of the chip. a, Schematic of the chip. **b**, Working principle, illustrating the intensity of the incident light, $I(\lambda)$, and the intensities of the reflected light from the reference area, $I_{r\_Ref}(\lambda)$, and from the centre of the membrane, $I_{r\_Centre}(\lambda, P)$. Insets: mechanical deformation of the membranes with and without applied pressure, P (right and left panels, respectively). **c**, Schematic of chip fabrication, at two stages. Top: poly-silicon layer Poly1 defines the bottom membrane; two sacrificial silicon oxide layers, Ox3 and Ox2, define the Fabry–Pérot cavity; two poly-silicon layers, Poly2 and Poly3 (Poly3 shown in bottom panel), define the top membrane. Patterning of the poly1, poly2 and poly3 layers delimits the device. Devices were released by etching of the silicon oxide layer *Ox1* (not shown). **d**, Scanning electron microscopy image of the fabricated device. Scale bar, 3 µm. **e**, Theoretical displacement of the membrane, $Displ_{memb}$, versus membrane thickness t_{memb} and P (inset). **f**, Schematic of the optical multilayer structure defining the Fabry–Pérot resonator (n, refractive index; t, layer thickness). **g**,**h**, Simulated results of the reflection as a function of λ (**g**) and t_{gap} (**h**) for a multilayer structure comprising medium, 50-nm-thick poly-silicon layer, vacuum gap, 50-nm-thick poly-silicon layer, medium.

Supplementary Movie S1) and disappeared when cells were returned to normal culture conditions (Supplementary Fig. S7). Sensor-containing HeLa cells, with or without vacuoles, divided normally (Fig. 3c, Supplementary Movie S2), displayed active mitochondria (Supplementary Fig. S7) and were healthy 9 days later (Supplementary Fig. S8). We also confirmed that the pH of the vacuoles oscillated between 4 and 6, and that the internalized devices were not degraded inside the HeLa cells 9 days after lipofection (Supplementary Fig. S8). This result is in good agreement with the finding that poly-silicon did not degrade in solutions buffered at pH values between 4 and 9 (Supplementary Fig. S8).

We next analysed the mechanical transmission of extracellular pressure to a subcellular component. The presence of a sensor inside a vacuole has several inherent advantages. First, it can give information about how an external pressure is transmitted mechanically to organelles. Second, it prevents the eventual existence of mechanical cross-sensitivity on the devices because of other organelles or cytoskeletal filaments, which can induce small forces and displacements (Supplementary Fig. S2). Third, better-quality CLSM images are obtained when the sensors are immersed in a medium with a uniform refractive index (Supplementary Fig. S9). Figure 4a presents overlaid images of transmitted light and laser channels in which the vacuole and different parts of the device can be easily recognized. An external pressure was applied from 0 to 1 bar and from 1 to 0 bar. A comparison between I_{r_Sensor} inside the vacuole and for the calibrated sensor in air showed close proportional changes (Figs 4b and 2b) and confirmed that the extracellular pressure is transmitted into the vacuole (Supplementary Fig. S10). The results in Fig. 4c demonstrate the capability of detecting pressure fluctuations inside a cell. The reflection from the sensor depends on the optical properties of the surrounding media; however, the position of the resonance is almost invariant (Supplementary Fig. S11). We also observed that I_{r_Sensor} is reversible, demonstrating that the pressure inside the

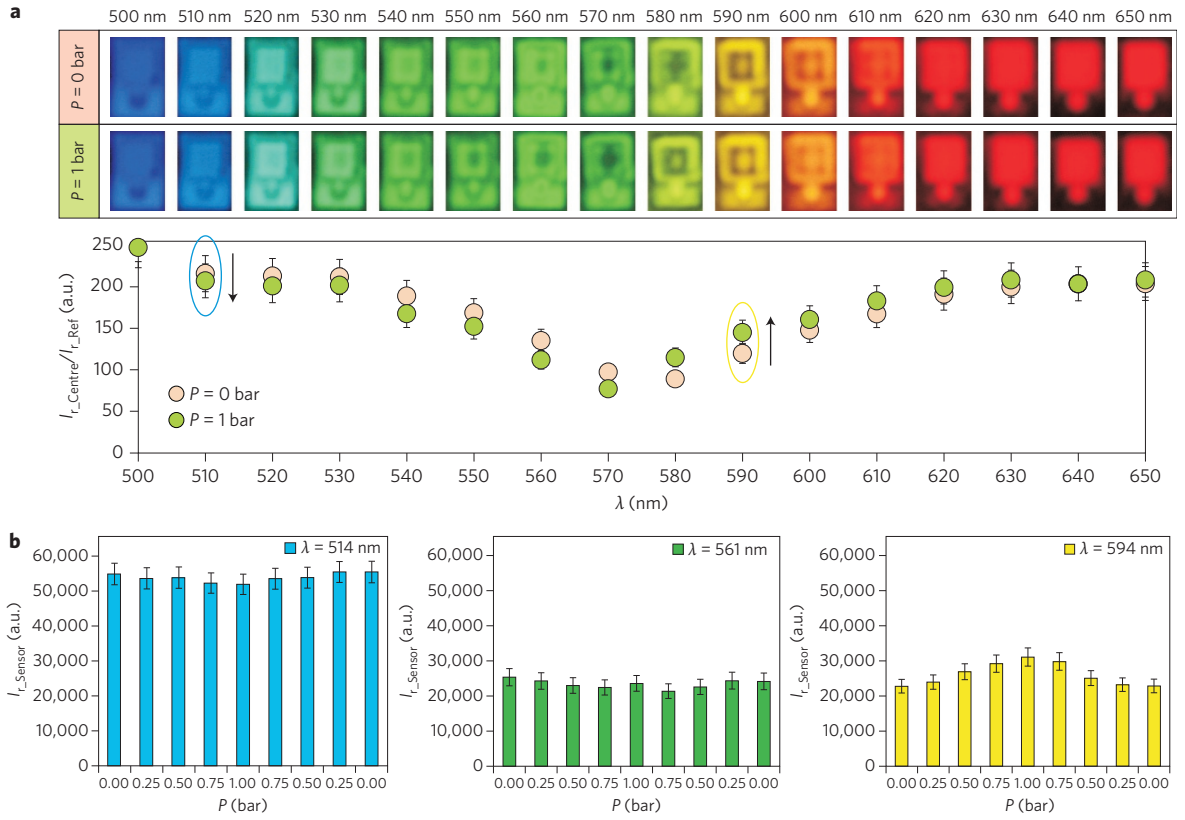

Figure 2 | Validation of the sensing principle. a, Bright-field optical microscopy experiment in air medium. Top: experimental true-colour images taken by an eight-bit colour CCD camera versus λ and P. Band-pass filters from 500 to 650 nm were used to select the working λ. Bottom: normalized I_{r_Centre}/I_{r_Ref} (255 a.u. for $\lambda = 500$ nm). P induces a lateral displacement of the curve towards smaller λ. For fixed λ, positive or negative sensitivities are observed (black arrows). Ovals indicate light colour ($\lambda = 510$ nm, blue; $\lambda = 590$ nm, yellow). Error bars, $\pm$10% (based on measurement uncertainty from images). **b**, CLSM experiment in air medium: I_{r_Sensor} versus P from 16-bit images. Lasers with $\lambda = 514$ nm, 561 nm and 594 nm were used to select the working λ. Positive and negative sensitivities are also observed for $\lambda = 594$ nm and $\lambda = 514$ nm, respectively. I_{r_Sensor} decreased for $0 \leq P \leq 0.75$ bar and increased for $P = 1$ bar, $\lambda = 561$ nm, as this is close to the resonance valley of the Fabry–Pérot spectrum. Error bars, $\pm$5%, 9% and 8% for $\lambda = 514$ nm, 561 nm and 594 nm, respectively (based on measurement uncertainty from images).

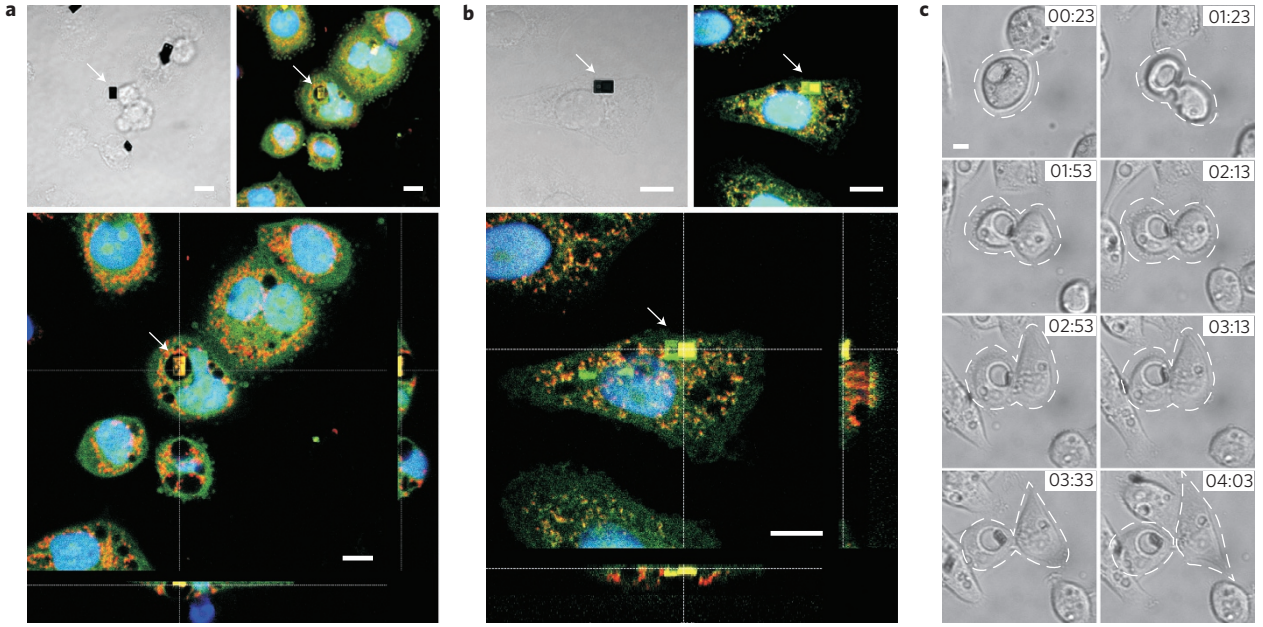

Figure 3 | Silicon chips inside human cells. a,**b**, A HeLa cell displaying an internalized chip (white arrow) inside a vacuole (**a**) and inside the cytoplasm (**b**). The cells were loaded with vital dyes CellTracker Green and MitoTracker Red before fixation. Top left: transmitted visible light image. Top right: overlay of confocal images. Bottom: orthogonal projection of confocal images showing that the chip is inside the cell. **c**, A HeLa cell containing a device inside the vacuole can proceed through mitosis (individual frames taken from Supplementary Movie S2; the time format is hh:mm). Scale bars, 10 μm.

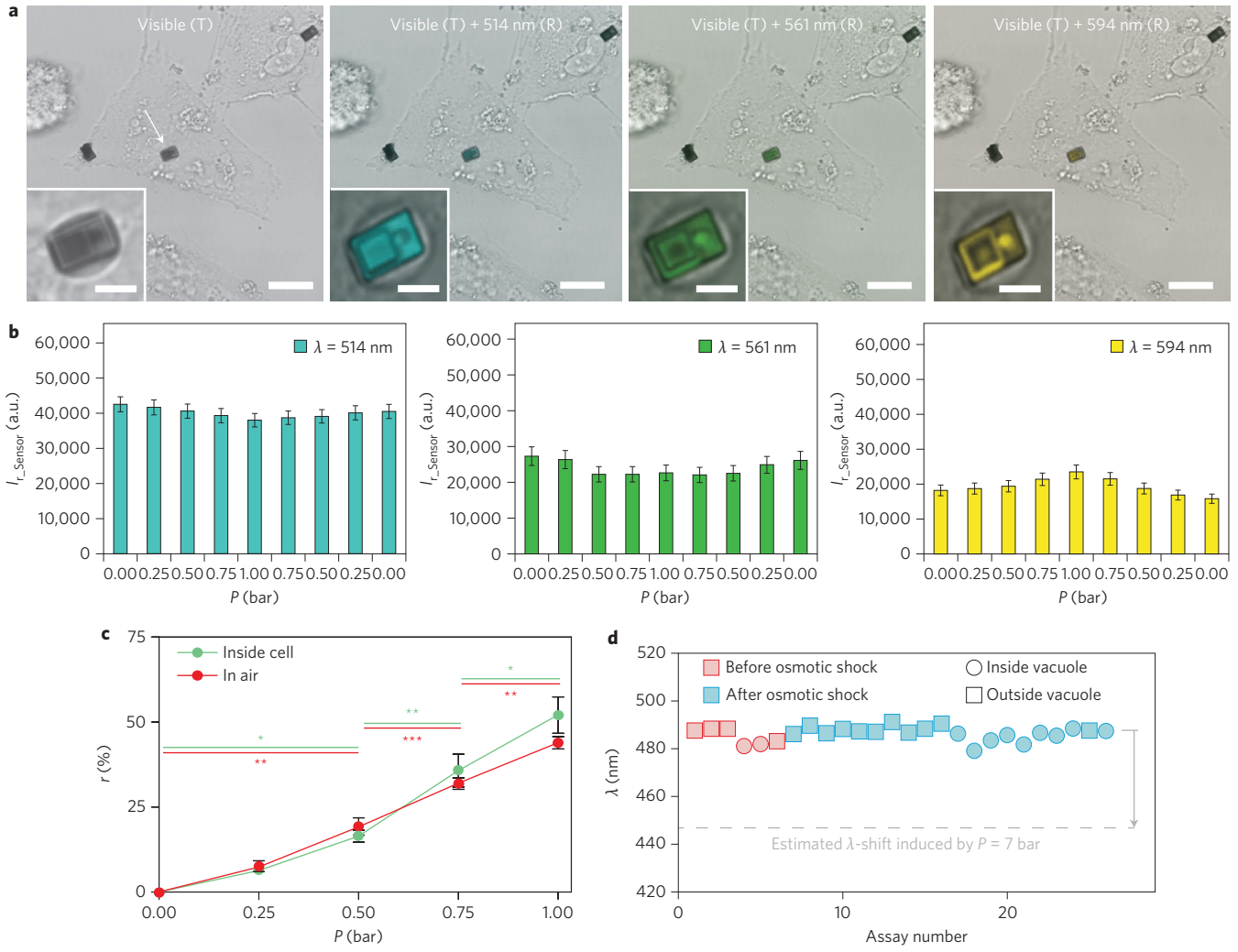

Figure 4 | Detection of pressure changes inside cells. a, False-colour 16-bit CLSM images of HeLa cells with a chip inside a vacuole (white arrow). Left to right: images show the cells under transmitted visible light and the reflected light of selected lasers ($\lambda = 514$, 561 and 594 nm). Insets: the chip inside a vacuole. Scale bars, 20 μm (main images); 5 μm (insets). **b**, I_{r_Sensor} versus P. Error bars, ±5%, 9% and 8% for $\lambda = 514$ nm, 561 nm and 594 nm, respectively (based on measurement uncertainty from images). **c**, Graph showing $(r) = (I_{r\_Sensor}(P, \lambda = 594\text{ nm})/I_{r\_Sensor}(P, \lambda = 514\text{ nm}))/(I_{r\_Sensor}(P = 0, \lambda = 594\text{ nm})/I_{r\_Sensor}(P = 0, \lambda = 514\text{ nm}))^{-1}$ for chips in air and inside cells. Statistical analysis: $^*P < 0.05$; $^{**}P < 0.01$; $^{***}P < 0.001$ (ANOVA, Bonferroni test). No significant differences were found between the chips' performance in air and inside cells (χ^2 test, $P = 0.6922$). Data are presented as the mean ± s.e.m. of five independent observations. **d**, Extrapolated λ for the minimum reflection of chips in the cytosol and inside the vacuole before and after an osmotic shock, showing a non-significant shift of the reflected spectrum after the shock.

vacuole follows extracellular pressure changes. This result shows that cross-sensitivities are not relevant (Supplementary Figs S4,S12).

We then analysed the effect of the exposure of HeLa cells to an osmotic shock (1/10 water dilution of the standard cell medium). A new batch of chips was fabricated for this study that showed a minimum reflection of the spectrum at 490 nm. The induced osmotic pressure predicted by van't Hoff's law is expected to produce a hydrostatic pressure of ~7 bar inside the cell. Accordingly, the predicted osmotic shock pressure should shift the Fabry–Pérot resonator minimum reflection by ~42 nm. Chips located both in a subcellular compartment (vacuole) (Supplementary Fig. S13) and in the cytosol of HeLa cells demonstrated that the reflection profiles of chips inside cells before and after the osmotic shock were practically the same (Supplementary Fig. S14). The extrapolated wavelength for the minimum reflection was very similar in all cases (Fig. 4d). We could infer that the pressure change inside the cell should be below a few hundreds millibars. Thus, our results provide direct evidence of low intracellular hydrostatic pressure when HeLa cells are submitted to a great osmotic stress.

Extracellular pressure is a common load in many real situations. Human cells experience $\Delta P = 0.2$ bar from feet to head, which can increase during human activity, and deep-sea animals can be exposed to 200 bar upon diving[19]. Hard-wire tensegrity models postulate that the cytoskeleton can resist mechanical forces[20]. Our experiments support the supposition that the cytoskeletons of human HeLa cells do not mechanically withstand extracellular pressures in the studied range and under our experimental cell-culture conditions. Thus, extracellular pressure is transmitted through the cytosol to the inner compartments. The implication is that intracellular transmission of fluid pressure follows Pascal's law. Our data also show that the intracellular pressure remains practically unaltered inside the cytosol and vacuoles during an osmotic shock, supporting the fact that these cells prevent the inward flow of water across their membranes[21]. Typically, when animal cells endure an osmotic shock they adapt, and do not experience a dramatic increase in intracellular pressure[22–24].

Additional work remains to be carried out to increase the sensitivity of the device so as to obtain accurate pressure measurements;

such further developments include thinner mechanical layers, auto-focus and tilt-stage systems, and computer-assisted measurements. Mechanical forces are not very well understood and are involved in basic cellular processes such as cell migration[25,26], diseases[27–29] and development[30]. Intracellular mechanical sensors will provide information directly from inside the cellular environment about these cellular forces and will provide new opportunities. We believe that this is a first step towards a wide-ranging field of intracellular nanochips that will offer a different perspective on fundamental problems in cell biology.

Methods

Imaging acquisition during pressure experiments. For Bright-field optical microscopy, experiments were performed with an Eclipse ME600 upright optical microscope (Nikon). A ×100 magnification, 0.8 NA, long-distance objective LU Plan ELWD 3.5 (Nikon) was used. Images were recorded using an 8-bit colour CCD (charge-coupled device) camera (DXM1200F, Nikon) using the advanced control software Nikon ACT-1 (Automatic Camera Tamer). Band-pass filters (Thorlabs) coupled with a YM-NCB11 filter slider (Nikon) were used to select the wavelength of the incident light.

For CLSM, confocal images were acquired with a confocal Leica TCS-SP5 microscope (Leica Microsystems GmbH), using 514 nm, 561 nm and 594 nm excitation laser wavelengths (acousto-optical tunable filters (AOTF) = 1%) for the first batch of fabricated chips, and 458 nm, 476 nm, 488 nm, 496 nm and 514 nm excitation laser wavelengths (AOTF = 1%), for the second batch of fabricated chips. The confocal analysis was conducted in the acousto-optical beam splitters (AOBS) reflection mode, with 16 bit-depth resolution and in the X–Y–Z scan mode. A ×63/0.9 HCX APO water objective (Leica Microsystems GmbH) was used. The image acquisition time was ~25 s. The images were pre-analysed by LAS AF software (Leica Microsystems GmbH).

Cell manipulation and osmotic shock. Chips were lipofected inside human HeLa cells using a protocol we have described previously[16]. HeLa cells were incubated for 12–16 h in the lipofection medium. Cell viability was analysed by incubating cells with Cell Tracker Green and MitoTracker Red (Molecular Probes, Invitrogen) for 15 min at 37 °C. HeLa cells were fixed with 4% paraformaldehyde in PBS for 45 min. The nuclei were stained with DAPI (Molecular Probes) and the cells were mounted with Fluoromont-G (Southern Biotech) for microscopy. HeLa cells were also incubated with Calcein AM, MitoTracker Red, DiOC and Lysosensor Red (Molecular Probes, Invitrogen), for direct observation under the CLSM following the manufacturers' recommendations. Cells were grown on glass coverslips and observed under the CLSM inside a live-imaging Ludin chamber. To expose cells to an osmotic shock, standard DMEM medium with 10% fetal bovine serum (Molecular Probes, Invitrogen) was 10% diluted in deionized water and perfused in the Ludin chamber.

Cell viability imaging. Cells were observed under a TCS SP2 AOBS CLSM with ×63 oil immersion lens (Leica Microsystems GmbH). Green fluorescence was monitored with excitation and emission settings of 488 nm and 505–550 nm, respectively. Red fluorescence was monitored with excitation and emission settings of 561 nm and 580–610 nm, respectively. A 351 nm laser line was used to image nuclei, and fluorescence emission was measured at 415–460 nm. Chips were imaged with a 488 nm laser line and they were detected by reflected light at 480–495 nm. Time-lapse microscopy was performed with a Leica AF6000 LX model DMI6000B, and pictures were taken every 10 min. HeLa cell videos were processed with Leica imaging software.

Statistical analysis. Data analysis was performed with Graph Pad Prism 4 software. Analysis of variance (ANOVA) and a Bonferroni test were used to compare intra-group data ('chip inside cell' or 'chip in air' data sets), and the χ^2 test was used to compare pressure data from calibration chips in air versus chips inside cells.

Extrapolate λ for minimum reflection. Values of λ for the minimum reflection (Fig. 4d) were extrapolated from data (Supplementary Fig. S14) by adjusting the mean intensities for the five selected lasers to a second-order polynomial. The minimum corresponded to the λ where the first derivative of the function was zero.

Received 2 August 2012; accepted 24 May 2013;
published online 30 June 2013

References

1. Stewart, M. P. *et al.* Hydrostatic pressure and the actomyosin cortex drive mitotic cell rounding. *Nature* **469,** 226–230 (2011).
2. Rand, R. P. & Burton, A. C. Mechanical properties of red cell membrane. i. Membrane stiffness+intracellular pressure. *Biophys. J.* **4,** 115–135 (1964).
3. Strohmeier, R. & Bereiterhahn, J. Hydrostatic-pressure in epidermal-cells is dependent on Ca-mediated contractions. *J. Cell Sci.* **88,** 631–640 (1987).
4. Kelly, S. M. & Macklem, P. T. Direct measurement of intracellular pressure. *Am. J. Physiol.* **260,** C652–C657 (1991).
5. Whitesides, G. M. The 'right' size in nanobiotechnology. *Nature Biotechnol.* **21,** 1161–1165 (2003).
6. Singhal, R. *et al.* Multifunctional carbon-nanotube cellular endoscopes. *Nature Nanotech.* **6,** 57–63 (2011).
7. Tian, B. Z. *et al.* Three-dimensional, flexible nanoscale field-effect transistors as localized bioprobes. *Science* **329,** 830–834 (2010).
8. Arlett, J. L., Myers, E. B. & Roukes, M. L. Comparative advantages of mechanical biosensors. *Nature Nanotech.* **6,** 203–215 (2011).
9. Cross, S. E., Jin, Y. S., Rao, J. & Gimzewski, J. K. Nanomechanical analysis of cells from cancer patients. *Nature Nanotech.* **2,** 780–783 (2007).
10. Balaban, N. Q. *et al.* Force and focal adhesion assembly: a close relationship studied using elastic micropatterned substrates. *Nature Cell Biol.* **3,** 466–472 (2001).
11. Vaziri, A. & Gopinath, A. Cell and biomolecular mechanics *in silico. Nature Mater.* **7,** 15–23 (2008).
12. Fan, J. Y. & Chu, P. K. Group IV nanoparticles: synthesis, properties, and biological applications. *Small* **6,** 2080–2098 (2010).
13. Tasciotti, E. *et al.* Mesoporous silicon particles as a multistage delivery system for imaging and therapeutic applications. *Nature Nanotech.* **3,** 151–157 (2008).
14. Fernandez-Rosas, E. *et al.* Intracellular polysilicon barcodes for cell tracking. *Small* **5,** 2433–2439 (2009).
15. Novo, S. *et al.* A novel embryo identification system by direct tagging of mouse embryos using silicon-based barcodes. *Human Reprod.* **26,** 96–105 (2011).
16. Gomez-Martinez, R. *et al.* Intracellular silicon chips in living cells. *Small* **6,** 499–502 (2010).
17. Born, M. & Wolf, E. *Principles of Optics* 6th edn (Pergamon, 1980).
18. French, P. J. Polysilicon: a versatile material for microsystems. *Sens. Actuat. A* **99,** 3–12 (2002).
19. Myers, K. A., Rattner, J. B., Shrive, N. G. & Hart, D. A. Hydrostatic pressure sensation in cells: integration into the tensegrity model. *Biochem. Cell Biol.* **85,** 543–551 (2007).
20. Ingber, D. E. & Tensegrity I. Cell structure and hierarchical systems biology. *J. Cell Sci.* **116,** 1157–1173 (2003).
21. Borgnia, M., Nielsen, S., Engle, A. & Agre, P. Cellular and molecular biology of the aquaporin water channels. *Annu. Rev. Biochem.* **68,** 425–458 (1999).
22. Spagnoli, C., Beyder, A., Besch, S. & Sachs, F. Atomic force microscopy analysis of cell volume regulation. *Phys. Rev. E* **78,** 031916 (2008).
23. Finan, J. D. & Guilak, F. The effects of osmotic stress on the structure and function of the cell nucleus. *J. Cell Biochem.* **109,** 460–467 (2010).
24. Pietuch, A, Brückner, B. R. & Janshoff, A. Membrane tension homeostasis of epithelial cells through surface area regulation in response to osmotic stress. *Biochim. Biophys. Acta Mol. Cell Res.* **1833,** 712–722 (2013).
25. Tambe, D. T. *et al.* Collective cell guidance by cooperative intercellular forces. *Nature Mater.* **10,** 469–475 (2011).
26. Trepat, X. *et al.* Physical forces during collective cell migration. *Nature Phys.* **5,** 426–430 (2009).
27. DuFort, C. C., Paszek, M. J. & Weaver, V. M. Balancing forces: architectural control of mechanotransduction. *Nature Rev. Mol. Cell Biol.* **12,** 308–318 (2011).
28. Jaalouk, D. E. & Lammerding, J. Mechanotransduction gone awry. *Nature Rev. Mol. Cell Biol.* **10,** 63–73 (2009).
29. Fritsch, A. *et al.* Are biomechanical changes necessary for tumour progression? *Nature Phys.* **6,** 730–732 (2010).
30. Wozniak, M. A. & Chen, C. S. Mechanotransduction in development: a growing role for contractility. *Nature Rev. Mol. Cell Biol.* **10,** 34–43 (2009).

Acknowledgements

This work was supported by the Spanish Government grants TEC2009-07687-E, TEC2011-29140-C03-01 and SAF2010-21879-C02-01. P.V. was supported by Centro de Investigación Biomédica en Red de Diabetes y Enfermedades Metabólicas Asociadas–Instituto de Salud Carlos III (CIBERDEM-ISCIII). The authors thank M. Calvo of Centros Científicos y Tecnológicos–Universidad de Barcelona (CCiT-UB), M.T. Seisdedos (CIB), J. Monteagudo (Leica Microsystems S.L.) and D. Megias of Unidad de Microscopía Confocal-Centro Nacional de Investigaciones Oncológicas (CMU-CNIO) for their assistance with CLSM experiments and A. Bosch (CCiT-UB) for assistance with image processing. The authors also thank the cleanroom staff of IMB-CNM for fabrication of the chips.

Author contributions

All authors discussed the results and contributed to writing the manuscript. M.D., R.G-M. and J.E. conceived and guided chip fabrication. Optical design and analysis was carried out by K.Z. The biological experiments were performed by A.M.H.P. and P.V., designed by A.M.H.P. and E.J.d.l.R., and planned and coordinated by T.S. R.G-M. performed the experimental characterization of the chips as well as data analysis. J.A.P. conceived and directed the project.

Additional information

Supplementary information is available in the online version of the paper. Reprints and permissions information is available online at www.nature.com/reprints. Correspondence and requests for materials should be addressed to J.A.P.

Competing financial interests

The authors declare no competing financial interests.